Article published online: 2022-12-13

Cyclopenta[*c*]thiophene- and Diketopyrrolopyrrole-Based Red-Green-Blue Electrochromic Polymers

Sashi Debnath[a,1]
Ganesh Masilamani[b]
Abhijeet Agrawal[a,2]
Neha Rani Kumar[a,3]
Chandan Kumar[a]
Sanjio S. Zade* [a]
Anjan Bedi* [b]

[a] Department of Chemical Sciences, Indian Institute of Science Education and Research Kolkata, Mohanpur, West Bengal, 741246, India
[b] Department of Chemistry, SRM Institute of Science and Technology, Kattankulathur, Tamil Nadu, 603203, India
* sanjiozade@iiserkol.ac.in, anjanb@srmist.edu.in

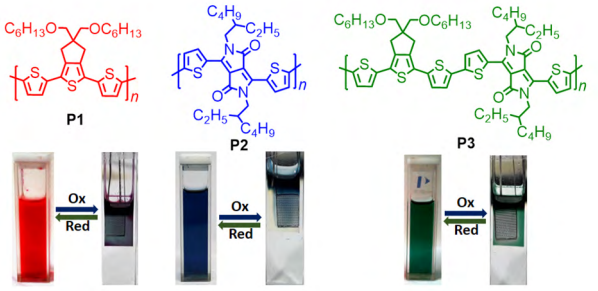

Received: 03.09.2022
Accepted: 09.11.2022
DOI: 10.1055/s-0042-1757979; Art ID: OM-2022-10-0041-OA

Abstract Cyclopenta[*c*]thiophene (CPT)-based polymers are potential candidates in organic electronics. Here, we report the first solution-processable red homopolymer (**P1**) of a thiophene-capped derivative of **CPT** (**DHTCPT**), and a blue homopolymer (**P2**) of N-substituted thienodiketopyrrolopyrrole (**DEHTDPP**). Additionally, by alternatingly copolymerizing the **DHTCPT** and **DEHTDPP** units, we achieved the green copolymer **P3**, thus completing the red-green-blue color wheels. We have shown experimentally and computationally (time-dependent density functional theory and natural bond orbital calculations) that **P1** and **P2** have very different optoelectronic features. However, in a donor–acceptor (D–A) copolymer **P3**, the optoelectronic properties have been tuned significantly to keep it in an intermediate range of **P1** and **P2. P2** and **P3** absorb throughout the whole UV-vis range of the solar spectrum. Furthermore, all polymers showed electrochromism to switch colors between neutral and polaronic states in solution. For **P1**, the maximum optical contrast (%Δ*T*) was observed for the SOMO→LUMO transition, whereas **P3** displayed the maximum %Δ*T* at the HOMO→LUMO transition.

Key words: conducting polymers, solution-processable, donor–acceptor polymer, electrochromicity, optical contrast

Introduction

π-Conjugated polymers (CPs) for organic electronic devices are important materials because of their potential advantages over inorganic and small organic molecules.[4] Several applications of CPs as active materials in polymer field-effect transistors (PFETs), polymer solar cells, polymer light-emitting diodes, sensors, and electrochromic devices have been the center of attention in the past few decades.[5,6] Their solution-processability, cost-effective synthesis, stability against aerial oxidation, amenable structural modifications and interesting structure–property relationships render them a major focus in organic chemistry.[7] Among these, a study on electrochromic CPs (ECPs) to complete the entire span of color palette received significant attention.[8] The general strategy in ECPs has been to synthesize polymers with the three primary colors of the red-green-blue (RGB) color wheel.[9] ECPs with these three primary colors showing high optical contrasts at different redox potentials are ideal candidates for electrochromicity-based applications.[10]

Covalently linked alternating donor (D) and acceptor (A)-based copolymers have been an efficient strategy to tune the optoelectronic properties in CPs.[11,12] For example, atomistic modification in the acceptor part efficiently tuned the optical bandgap (E_g^{opt}) to result in donor–acceptor (D–A) RGB polymers based on cyclopenta[*c*]thiophene (**CPT**) and benzazoles.[13,14] It is noteworthy to mention that even cyclopenta[*c*]chalcogenophene-based small molecules or polymers showed tunability of optoelectronic properties by atomistic modification.[15–18] However, in D–A alternating copolymers, **CPT**/thiophene-capped **CPT** (**TCPT**)-based oligomers (Figure 1) and benzazole are found to be an electron donor and electron acceptor, respectively, to result in D–A intramolecular charge transfer (ICT).[19] When the benzazole was replaced with dipyrromethene difluoroborane (BODIPY), a black polymer with E_g^{opt} of 1.28 eV was produced.[20] Alternate copolymers based on DCPT and thiophene showed descent hole mobility (1.4×10^{-2} cm$^2 \cdot$V$^{-1} \cdot$s^{-1}) in PFETs.[21] While most of the **CPT**-based polymers were found to be amorphous, copolymers based on **CPT** and bithiazole building blocks showed superior p-type hole mobility (~0.05 cm$^2 \cdot$V$^{-1} \cdot$s^{-1}) arising from the semicrystalline nature of the polymers.[22] The semicrystalline nature of the polythiophenes is known

to result in efficient inter-lamellar charge transport via hopping. This could also have a significant impact on ECPs, where a narrow switching time between the doped and de-doped states is required.[23] The coloration efficiency of the CPs is altered drastically by varying the π-backbones. One way to improve the semicrystalline nature of the polymers has been to synthesize copolymers, where the other building block carries multiple types of heteroatoms, which could lead to better inter-lamellar interactions in the solid state.[22]

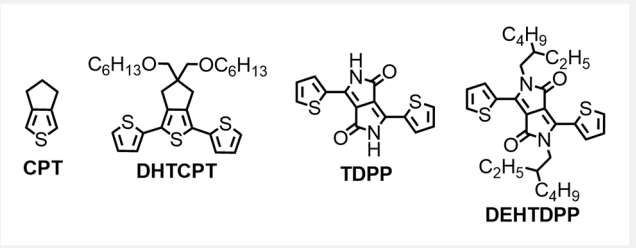

Figure 1 Structures of **CPT**, **TCPT**, **TDPP**, and **DEHTDPP**.

Contextually, 3,6-di(thiophen-2-yl)-2,5-dihydropyrrolo [3,4-*c*]pyrrole-1,4-dione (**TDPP**) has been a potent building block in organic electronics.[24] Minor synthetic modifications on **TDPP** derivatives or polymers provide access to improved ordering in solid-state packing and excellent charge transport properties.[25] Even a small chiral side chain on the **TDPP** unit can induce strong optical activity via hierarchical self-assembly in **TDPP**-based polymers.[26] The photophysical properties can be fine-tuned by structural modifications that lead to alterations in frontier molecular orbitals (FMOs). The ICT and π–π stacking facilitate the intra- and inter-chain hopping of charges in **TDPP**-based small molecules or polymers, resulting in superior ambipolar charge transport with a high on/off ratio ($I_{on/off}$).[25,27] Furthermore, the near-IR absorption of the **TDPP**-based polymers promises applications in electrochromic displays. However, there is only one report on the electrochromic behavior of the homopolymer of **TDPP**.[28]

Inspired by these, here we have synthesized a homopolymer of 2,5-bis(2-ethylhexyl)-3,6-di(thiophen-2-yl)pyrrolo [3,4-*c*]pyrrole-1,4(2H,5H)-dione (**DEHTDPP**) and the first solution-processable homopolymer of thiophene-capped 5,5-bis(hexyloxy)-5,6-dihydro-4H-cyclopenta[*c*]thiophene (**DHTCPT**) (Scheme 1). Additionally, we made the alternating copolymer based on **DHTCPT** and **DEHTDPP**. On the premise of the variations in the polymer backbone, this enabled us to investigate the optoelectronic and electrochromic properties of the resultant polymers.

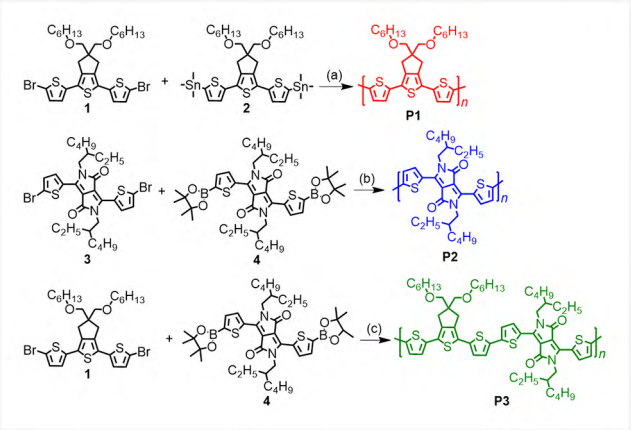

Scheme 1 Synthetic pathway to the polymers **P1**–**P3**. Conditions: (a) $Pd_2(dba)_3$, $P(o\text{-tolyl})_3$, toluene, 110 °C, 24 h; (b) $Pd(dppf)Cl_2$, Na_2CO_3, toluene/ethanol/water (2.5/1/1), 85 °C, 22 h; (c) $Pd_2(dba)_3$, $P(o\text{-tolyl})_3$, toluene, 110 °C, 28 h.

Results and Discussion

Synthesis and Characterization

The monomers **1**–**4** were synthesized according to the previously reported methods.[19,29] Generally, copolymerization of the **CPT**-based monomers was performed by Stille coupling, which could keep the polydispersity indices (PDIs) below 2. Additionally, the Stille coupling method afforded **CPT**-based polymers with reproducible device properties in terms of hole mobility and on/off ratio.[21] So, **P1** was synthesized by the Stille polymerization method[30] using **1** and **2**. Although **TCPT** was used to make many copolymers by us earlier, this is the first synthesis of its solution-processable homopolymer. **P2** (homopolymer of **DEHTDPP**) was synthesized by Suzuki polymerization of **3** and **4** as this method is known to produce highly efficient materials for electronic devices.[25,29] Here, the alternate copolymer **P3** was afforded by a Stille cross-coupling polymerization between **2** and **3**. Finally, the polymers were purified by Soxhlet extraction and precipitation from the chloroform extract using methanol as a non-solvent. The presented polymerization methods furnished the three polymers with yields ranging between 62% and 74% and PDIs in the range of 1.7–1.8 (Table 1). It can be noted that the homopolymers were obtained with slightly lower yield and molecular weight. M_n values of 11.3, 8.2 and 6.2 affirm the presence of at least 22,

Table 1 Physical properties of the polymers

Polymer	M_w (kD)	M_n (kD)	PDI	T_d (°C)
P1	19.2	11.3	1.67	251
P2	14.9	8.2	1.84	268
P3	11.0	6.2	1.7	224

15 and 6 repeating units of the corresponding monomeric or comonomeric units in **P1, P2**, and **P3**, respectively (Table 1). The polymers exhibited ample solubility for further solution-based studies. Decomposition temperature (T_d) was calculated at 5% thermal decomposition for the polymers. **P2** showed maximum stability with a T_d of 251 °C (see Figure S4 in the Supporting Information).

Optical and Electrochemical Properties

The polymer showed three basic colors of the RGB color wheel. **P1, P2** and **P3** displayed red, blue and green colors, respectively, in their chloroform solutions. This shows the importance of the alternating copolymer to complete the RGB spectrum of colors. **P1** showed one major absorption band around 526 nm, due to the π–π* transition (Figure 2). The HOMO–LUMO gap (HLG) calculated from the absorption onset of absorption (λ^{abs}_{onset}) was found to be 2.02 eV. This is in line with the previously synthesized thin films of the homopolymers by the electrochemical method.[17] Both **P2** and **P3** were found to show absorption spectra covering the UV-vis range with two significant bands. The **TDPP**-based oligomers are known to have a strong transition in the near-IR region due to ICT between the donor-type thiophene and the acceptor-type lactam unit. The **TDPP**-containing polymers are known to show similar behavior as well. As a result, the longer wavelength band in **TDPP**-based polymers originates from the ICT, and the π→π* transition appears at a lower wavelength. The wavelength of absorption maxima (λ_{max}) for **P2** appeared at 692 nm with two weaker peaks around 313 and 396 nm. Compared to other reported homopolymers of **TDPP** carrying different substitutions on N-atom, **P2** exhibited a lower λ_{max}, which may be due to a substitution effect or an effect of a shorter chain length of the polymer backbone.[25] But, ~140 nm red-shifted λ_{max} of **P2** compared to the **DEHTDPP** monomer[24] is evident of a significantly long polymeric chromophore in **P2**. The HLG calculated from the λ^{abs}_{onset} of the solution-state UV-vis spectra is 1.48 eV, the lowest among the current series. The alternate copolymer **P3** showed a strong transition at 678 nm and a weaker peak at 416 nm.

The electrochemical properties of the polymers were characterized by CV (Figure 3a). The polymers displayed peaks for both anodic oxidation and cathodic reductions. The oxidation of the polymers was irreversible. The onset of the oxidation (E^{ox}_{onset}) for **P2** was calculated to be 0.13 V higher than that of **P1**. The HOMO level was calculated to be located at −5.04 for **P1** and −5.17 eV for **P2.** The presence of the lactam unit is known to stabilize the HOMO in **DEHTDPP** homopolymers. Compared to this, incorporating more electron-rich thiophene in the alternating copolymer backbone is expected to destabilize HOMO. Evident to this conclusion is the E^{ox}_{onset} value of **P3** (0.64 V, HOMO = −5.08 eV), which is between the two extreme values of **P1** and **P2**. Under the cathodic voltage sweep, **P1** and **P2** showed irreversible behavior, whereas **P2** displayed a quasi-reversible reduction due to the presence of the lactam units. The trend in electrochemical reduction was the opposite in terms of the onset of the reduction (E^{red}_{onset}). E^{red}_{onset} for **P1** was 0.41 V higher than that of **P2**. However, alternating copolymer **P3** showed an intermediate E^{red}_{onset} value (−0.94 V) compared to **P1** and **P2**. The energy of the LUMO was calculated to be −3.32 and −3.67 eV for **P1** and **P2**, respectively. Thus, the electrochemical bandgap (E^{elec}_{g}) values of 1.72 and 1.5 eV were achieved for **P1** and **P2**, respectively. For completion of the RGB color wheel, intermediate FMO levels of the **P1** and **P2** were essential. By combining the **TCPT** and **DEHTDPP** units, we

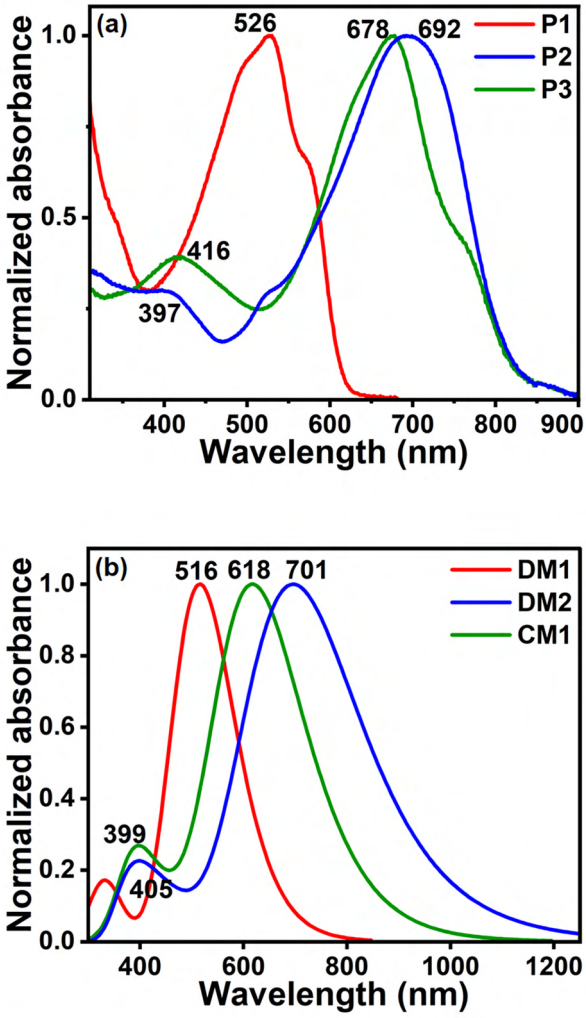

Figure 2 (a) Experimental UV-vis absorption spectra of the polymers in chloroform; (b) computational (TDDFT/B3LYP/6 – 31 G(d,p)) UV-vis absorption spectra of **DM1, DM2**, and **CM1**.

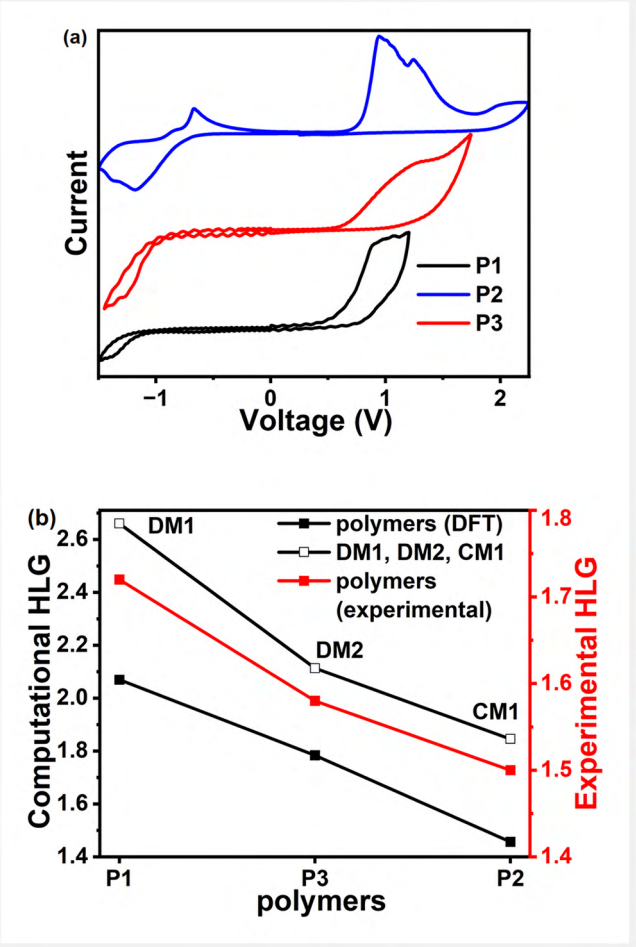

Figure 3 (a) CV of the polymers in acetonitrile as a solvent and tetrabutylammonium hexafluorophosphate ($TBAPF_6$) as an electrolyte; (b) experimental (electrochemical) and computational (DFT/6–31 G(d,p)/B3LYP) bandgap in the polymers, model dimers, and comonomers.

were able to achieve **P3**, which has intermediate properties of the FMOs (HOMO = −5.08 eV; LUMO = −1.58 eV) compared with individual homopolymers **P1** and **P2**.

Density functional theory (DFT/B3LYP-6–31 G(d,p)) was used to optimize the polymers in order to thoroughly examine the nature of the electronic transition, FMOs, and electrochemical characteristics (see Figure S6 in the Supporting Information). Generally, time-dependent DFT (TDDFT) studies are conveniently performed upon the gas-phase optimized geometry. So, the model comonomer for **P3** (**CM1**) and the dimers for **DHTCPT** (**DM1**) and **DEHTDPP** (**DM2**) were optimized (see Figure S5 in the Supporting Information) using DFT (DFT/B3LYP-6–31 G(d,p)) and TDDFT calculations were performed at the same level of computations. The optimized geometry of the polymers was found to be nearly planar. Computationally obtained results (Figure 3b) complemented multiple experimental observations. **DM1, DM2** and **CM1** displayed planarity in the gas-phase optimized geometry. The electron density in the HOMO and LUMO for DM1 was delocalized all over the polymer backbone (Figure 4). However, significant localization of electron density in **DM2**'s HOMO and LUMO was seen over lactam rings, indicating a key role for those in regulating the energies of the FMOs. In **DM1**, the transition at 516 nm could be related to the electronic transition of **P1** at 526 nm. This peak is clearly due to π→π* transition within the HOMO→LUMO (f = 1.9341) levels. In **DM2**, the HOMO→LUMO (f = 1.7182) transition was calculated at the longest wavelength (701 nm) among the three. This can be compared to the peak at 692 nm for the **P2**. Interestingly, the D–A copolymer **P3** showed this transition at 678 nm in solution, which can be correlated well to the peak at 618 nm (f = 1.6278) for **CM1**. The peaks at a shorter wavelength for **P2** and **P3** in a solution can be compared to those of **DM2** and **CM1** studied at gas-phase calculation. For **DM2**, the band at 405 nm (f = 0.2635) consisted of two major transitions from HOMO−2→LUMO (46%) and HOMO→LUMO+2 (37%), which can be correlated to the band at 397 nm for **P2**. Similarly, for **CM1**, the band at 399 nm (f = 0.2269) arising from a combination HOMO−1→LUMO+1 (66%) and HOMO→LUMO+2 (22%) of two transitions can be correlated to the band at 405 nm for **P3**. The computed gap between the highest occupied crystal orbital and lowest unoccupied crystal orbital of 2.07, 1.78 and 1.45 eV for **P1, P2**, and **P3,** respectively, reflects the trend in both E_g^{opt} and E_g^{elec}.

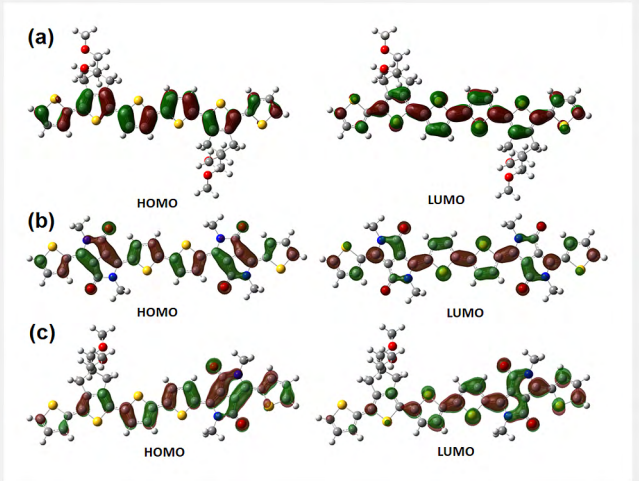

Figure 4 Contour maps of the HOMO and LUMO of the optimized (DFT/B3LYP/6–31 G(d,p) structures of (a) **DM1**, (b) **DM2**, and (c) **CM1** (isovalue = 0.025).

For further insight into the most critical electron delocalization pathways, which are responsible for the stabilization of the molecules, natural bonding orbital (NBO) analyses were performed on **DM1, DM2**, and **CM1** at the 6–31 G(d,

p)/M06 – 2X level of theory (see Figure S8 and Table S2 in the Supporting Information). In **DM1**, the π-electron delocalization throughout the molecule provided stability. The most significant charge transfer which stabilizes the system is from the adjacent thiophene rings to the **CPT** moiety. The optimized structures of **DM2** and **CM1** displayed some distinct variations in the accumulation of charges over the lactam ring compared to other parts of the molecules. The primary ICT in **DM2** is from the lone pairs of electrons on N-atoms to the antibonding orbitals of the C=O bonds. This was also found with similar stabilization energies in the **CM1**. There were two crucial observations from the NBO calculations of **DM1** and **DM2** when compared independently to the **CM1**. Firstly, stabilization energy is associated with the charge transfer from the adjacent thiophene ring to the lactam ring. In **DM2**, the charge transfer was found between the antibonding orbital of C14 – C15 ($ED_i = 0.35702$) to C9–C10 ($ED_j = 0.39688$) with stabilization energy (E^2) of 324.41 kcal/mol). However, E^2 within identical NBOs in **CM1** was remarkably decreased by 127.49 kcal/mol BD* of C14 – C15 ($ED_i = 0.37067$) to BD* of C9–C10 (EDj = 0.38225), $E^2 = 196.92$ kcal/mol). Secondly, E^2, arising from the charge transfer from the thiophene ring to the **CPT** ring in **CM1,** is reduced by 43.18 kcal/mol ((BD* of C43 – C48 ($ED_i = 0.02064$) to BD* of C37 – C41 ($ED_j = 0.34568$), $E^2 = 147.87$ kcal/mol)), compared to E^2 for charge transfer within identical NBOs in **DM1** ((BD* of C52 – C57 ($ED_i = 0.34950$) to BD* C46 – C49 ($ED_j = 0.3530$), $E^2 = 191.05$ kcal/mol)). So, the combination of **TCPT** and **DEHTDPP** in an alternate fashion resulted in a delicate balance to keep the intermediate stabilization energies of the NBOs compared to their individual components. Also, in contour maps of the LUMO of **CM1**, a significant localization of the electron density over the **TDPP** unit could be attributed to significant ICT. Similar phenomena could be expected for the polymers comprising the **DM1, DM2**, and **CM1** as repeating units. It was very important to achieve the energies of the FMOs for the **P3** as an intermediate of **P1** and **P2** to achieve a variable band gap and to achieve the RGB color wheel.

Spectroelectrochemistry and electrochromicity

To fully utilize the potential of the spectral and electrochemical profile of the polymers, spectroelectrochemistry was performed in an oxidative manner. The spectroelectrochemical behavior of the molecules was studied in the absorption range of 300 – 1600 nm to study the electrochromism of the polymers and the singly charged polarons. **P1, P2**, and **P3** were studied under potential windows of 0.1 – 0.8, 0.1 – 0.9 and 0.3 – 0.9 V, respectively (Figure 5). **P1** changed color from red to transparent blue when switched reproducibly between 0.1 and 0.8 V. Similarly, **P2** (under 0.1 – 0.9 V) and

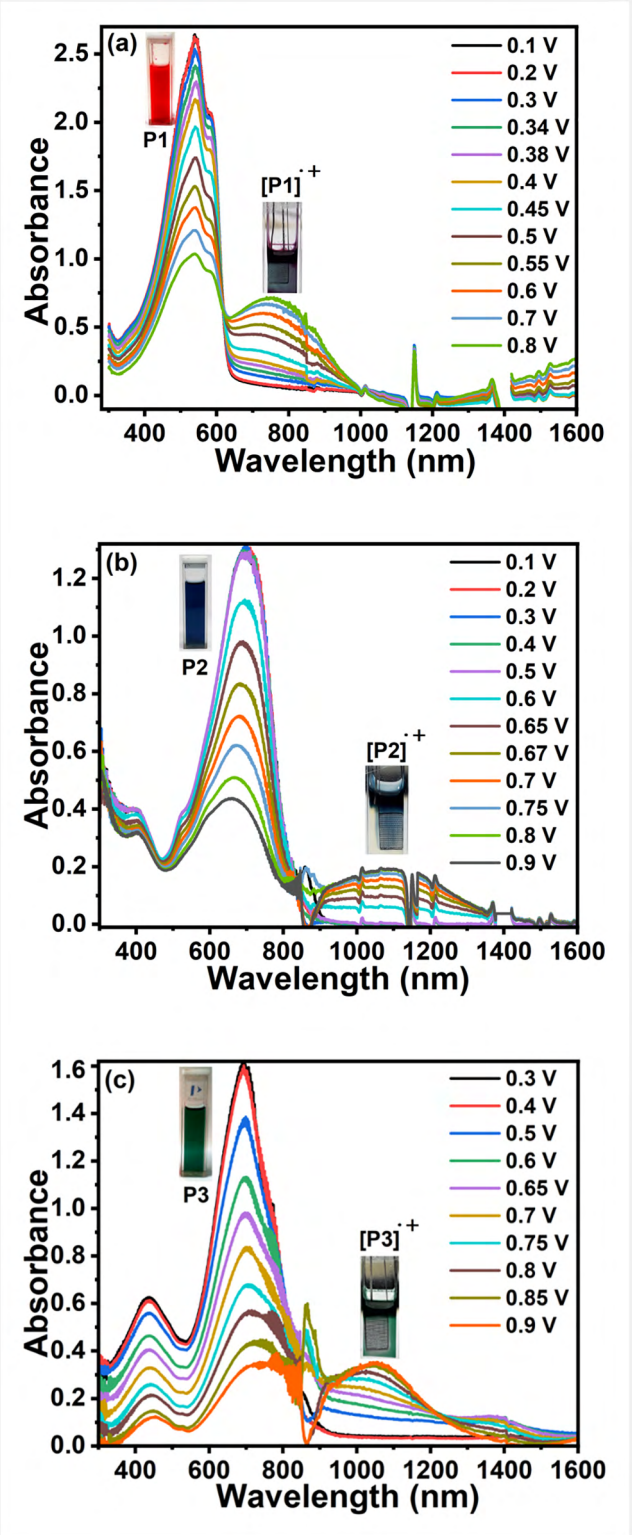

Figure 5 Spectroelectrochemistry of (a) **P1**, (b) **P2**, and (c) **P3** in dichloromethane solution using $TBAPF_6$ as an electrolyte.

P3 (0.3 – 0.9 V) exhibited the reproducible color transitions, blue→transparent and green→transparent, respectively. Upon gradual oxidation, the intensity of the peak at λ_{max} for **P1** faded, while the polaronic absorption band originating from singly charged polymer (**P1**$^{\bullet+}$) started appearing at a higher wavelength and intensified further with an increase in potential and saturates after 0.8 V.

For **P2**$^{\bullet+}$ and **P3**$^{\bullet+}$, the absorption peaks were observed at 1015 and 1057 nm, respectively. In spectroelectrochemistry, the polymers showed one clear isosbestic point between the peaks related to absorption from the neutral polymer and polaron. The appearance of this isosbestic point indicates the transformation of the polymer chain into only one other species in solution, which is polaron. There may be the formation of bipolaron in an interim applied potential, but the limitation in the measurement window[31] of the used UV-vis spectrophotometer restricted us from further discussion.

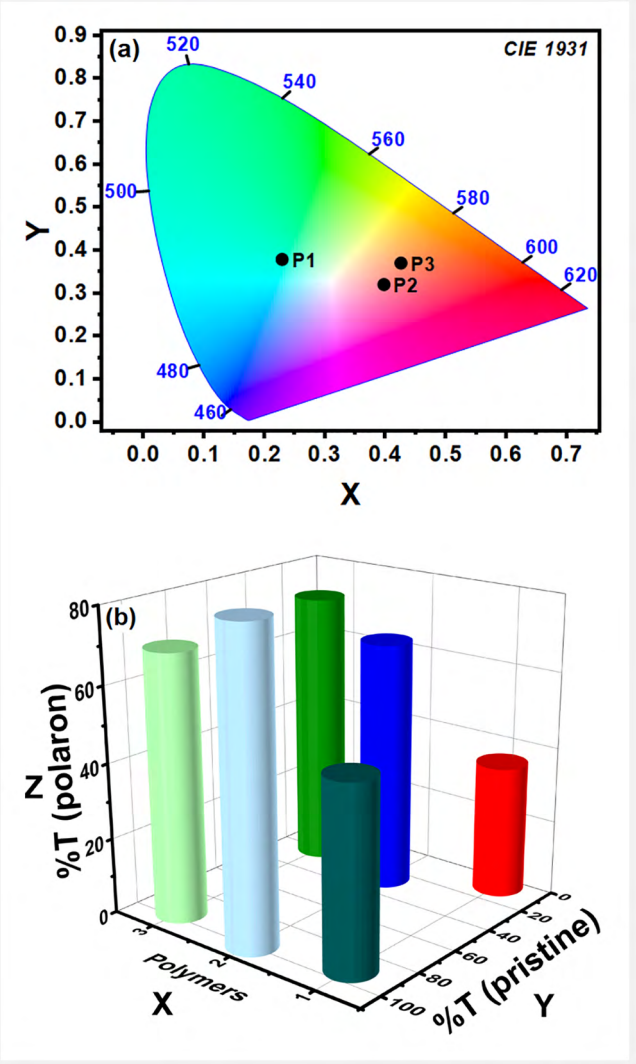

Figure 6 (a) CIE color coordinates 1931 (2° observer) for **P1**-0.23 (*x*), 0.38 (*y*), **P2**-0.40 (*x*), 0.32 (*y*) and **P3**-0.43 (*x*), 0.37 (*y*) are obtained from absorption spectra of the polymers in chloroform. (b) Change in %*T* values of the polymers during spectroelectrochemistry. On the *XY* plane, the bottom of the pillars represents the initial values of %*T*, and the *Z*-axis represents the final values of %*T* of the polymers. The frontal and rear pillars represent %*T* values for SOMO→LUMO and HOMO→LUMO transitions, respectively. *X*-axis: polymers 1 (**P1**), 2 (**P2**), and 3 (**P3**).

The chromaticity diagram for the polymers represents the variety in the visual appearance of the polymers in neutral states (Figure 6a). The polymers showed a range of optical contrasts in different wavelengths (Figure 6b). The %Δ*T* values recorded at the HOMO→LUMO transition from the undoped polymer solution and singly occupied molecular orbital (SOMO)→LUMO transition from the polaronic species are summarized in Figure 6b. **P1**, which changed color from red to transparent blue upon oxidation, demonstrated a %Δ*T* of 29 and 44 arising from the change in optical density at the HOMO→LUMO and HOMO→SOMO transitions, respectively. Similarly, **P2** displayed %Δ*T* of 39 and 17 when measured at their major peaks due to neutral and polaronic states. In **P3**, %Δ*T* of 53 and 26 were found at the HOMO→LUMO and SOMO→LUMO transitions, respectively. We achieved 1.8 and 1.4 times higher %Δ*T* for the HOMO→LUMO transition in the UV-vis region for **P3**, compared to those of **P1** and **P2**, respectively, as well as decent %Δ*T* in the near-IR region, by alternately polymerizing the **DHTCPT** unit with the **DEHTDPP** unit in **P3**. It is non-trivial to correlate this to a particular reason for structurally different polymers, unlike other polymer backbones, where a single hetero atom changes the nature of conjugation.[32] Here, the ICT transition in both **P2** and **P3** in the D–A alternating copolymer backbone is observed to be affected mainly through extrinsic doping.

Conclusions

In summary, we have synthesized three new soluble and thermally stable polymers based on **TCPT** and **DEHTDPP** by Pd-catalysed Stille and Suzuki coupling methods. **TCPT** and **DEHTDPP** afforded the red and blue polymers **P1** and **P2**, respectively, upon homopolymerization. In contrast, their copolymerization in an alternate fashion resulted in the green polymer **P3**. The HOMO level is the most stable in the case of **P2** and the least in the case of **P1**. The trend in LUMO energy is the opposite. The D–A copolymer **P3** possesses HOMO and LUMO energies in between those of the **P1** and **P2**. The computationally obtained contour maps of HOMO and LUMO of the **P3** show that the electron-rich **DHTCPT** controls the HOMO and the electron-deficient **DEHTDPP** units control the LUMO energy. DFT calculations supported the trends in HLGs from UV-vis spectra and CV. Additionally, NBO calculations hinted at the presence of several energy-stabilizing phenomena in the dimer model of the polymers. The ICT

from the thiophene to the lactam ring in **DEHTDPP** was found to be the dominating factor in the energy stabilization of the molecular orbitals. Very importantly, the polymers displayed electrochromicity, measured at the solution state. The most significant %Δ*T* of 53 was obtained for the copolymer **P3**, compared to the homopolymers at the λ_{max} of the HOMO→LUMO transition. However, **P1** showed the most superior %Δ*T* of 44 in the case of the SOMO→LUMO transition. So, the judicial design of **CPT-** and **TDPP**-based polymers could furnish materials for tunable optoelectronic properties and color-switching abilities in relevant future devices.

Experimental Section

Most of the reagents and solvents obtained from commercial sources were used without any further purification. Reagent-grade toluene was dried over sodium. NMR spectra were recorded on a Bruker AVANCE 500 FT-NMR spectrometer using $CDCl_3$ as the solvent and chemical shifts are reported in parts per million (δ scale) relative to TMS as the internal standard. Column chromatography was performed using silica gel (100 – 200 mesh). Molecular weight and polydispersity of the polymers were obtained from gel permeation chromatography (GPC, Waters 2414) analyses against polystyrene standard using THF at a flow rate of 0.3 mL/min at r.t. Thermogravimetric analysis (TGA) was performed on a Mettler Toledo TGA/SDTA 851 analyzer at a heating rate of 10 °C·min^{-1} under nitrogen. UV-vis-NIR spectra of the polymers were recorded on a HITACHI U-4100 UV-vis-NIR spectrophotometer in polymer solutions having concentration of 0.15 mg/mL. Electrochemical analysis was carried out with a Princeton Applied Research 263A potentiostat using a platinum (Pt) disk electrode as the working electrode, a platinum wire as the counter electrode, and an AgCl-coated Ag wire as the reference electrode. Pt disk electrodes were gleamed with alumina, water, and acetone and were dried under nitrogen flow to remove any incipient oxygen. 0.1 M tetrabutylammonium hexafluorophosphate ($TBAPF_6$) in dichloromethane (DCM) was used as an electrolyte. Films were drop-cast on a Pt-disk electrode for CV. In situ spectroelectrochemistry was performed by synchronizing the operations on the potentiostat and UV-vis spectrophotometer, simultaneously. Spectroelectrochemistry of the polymers was recorded in 0.75 mg/mL DCM solution of the polymers using 0.1 M $TBAPF_6$ as an electrolyte and a Pt-mesh electrode (5 mm × 8 mm) as the working electrode.

Procedures

*Synthesis of **P1***. To an oven-dried 50 mL two-neck round-bottom flask under nitrogen was added dry toluene (10 mL) along with **2** (100 mg, 0.1190 mmol) and **1** (80 mg, 0.1190 mmol). The resulting solution was purged with dry nitrogen for 20 min. $Pd_2(dba)_3$ (11 mg, 0.0119 mmol) and P(*o*-tolyl)$_3$ (18 mg, 0.0595 mmol) were added into the flask. The reaction mixture was stirred at 110 °C under a nitrogen atmosphere and was monitored with thin layer chromatography. The reaction vessel was cooled to r.t. after 24 h and cold methanol was added to the reaction mixture to find dark red precipitate. The precipitate was collected by filtration on a Whatmann®42 filter paper and was washed sequentially with methanol and acetone in a Soxhlet extraction apparatus for 28 h until the wash solution was colorless and then extracted by chloroform. To the chloroform fraction, methanol was added and the resulting precipitate was filtered. The residue was dried under vacuum (10^{-2} bar) to afford the red polymer **P1** (46 mg, 74%).

^{1}H NMR (400 MHz, $CDCl_3$): δ 7.00 (br), 3.48 (br), 2.79 (br), 1.33 – 1.25 (br, 4 H), 0.89 (br).

GPC (THF, 298 K, polystyrene standard): M_w = 19,200 Da, M_n = 11,300 Da, and PDI = 1.67.

UV-vis ($CHCl_3$): 526 nm.

*Synthesis of **P2***. **3** (100 mg, 0.1470 mmol), **4** (114 mg, 0.1470 mmol), Pd(dppf)Cl_2 (10 mg, 0.0147 mmol), and Na_2CO_3 (155 mg, 1.4700 mmol) were taken in a 100 mL Schlenk flask, and the flask was evacuated and back-filled with argon three times. A degassed solvent mixture consisting of toluene (25 mL), ethanol (9 mL) and water (10 mL) was transferred to the Schlenk flask through a septum. The reaction mixture was purged with argon for 15 min. The reaction was carried out at 85 °C for 22 h under an argon atmosphere resulting in blue precipitates on the wall of the flask. There was added a 50 mL solvent mixture containing methanol/water (1/1) to complete the precipitation from the reaction mixture. After completion of the precipitation, the resulting reaction mixture was filtered through a Whatmann®42 filter paper. The residue was washed with methanol and acetone to confirm removal of catalyst residues and short oligomers. Finally, the Soxhlet extraction method using chloroform was performed and the concentrated polymer solution (~20 mL) was poured slowly into 250 mL of cold methanol under vigorous stirring. After 15 min of stirring, polymer was collected by vacuum filtration and dried under vacuum (10^{-2} bar) to afford the blue polymer **P2** (99 mg, 69%).

^{1}H NMR (400 MHz, $CDCl_3$): δ 9.01 – 8.92 (br), 7.59 – 7.09 (br), 4.03 (br), 1.89 (br, 4 H), 1.38 – 1.25 (br), 0.89 (br).

GPC (THF, 298 K, polystyrene standard): M_n = 14,900 Da, M_w = 8,200 Da, and PDI = 1.84.

UV-vis ($CHCl_3$): 397, 692 nm.

Synthesis of ***P3***. To an oven-dried 50 mL two-neck round-bottom flask under nitrogen was added dry toluene (10 mL) along with **2** (100 mg, 0.1190 mmol) and **3** (81 mg, 0.1190 mmol). The resulting solution was purged with dry nitrogen for 20 min. $Pd_2(dba)_3$ (11 mg, 0.0119 mmol) and P(*o*-tolyl)$_3$ (18 mg, 0.0595 mmol) were added into the flask. The reaction mixture was stirred at 110 °C under a nitrogen atmosphere and was monitored with thin layer chromatography. The reaction vessel was cooled to r.t. after 28 h and cold methanol was added to the reaction mixture to find dark red precipitate. The precipitate was collected by filtration on a Whatmann®42 filter paper and was washed sequentially with methanol and acetone in a Soxhlet extraction apparatus for 28 h until the wash solution was colorless, followed by extraction with chloroform. To the chloroform fraction, methanol was added and the resulting precipitate was filtered. The residue was dried under vacuum (10^{-2} bar) to afford the green polymer **P3** (76 mg, 62%).

^{1}H NMR (400 MHz, $CDCl_3$): δ 8.98 (br), 4.04 (br), 3.45 (br), 2.77 (br), 1.94 (br, s), 1.62 (br, s), 1.31 (br), 0.88 (br).

GPC (THF, 298 K, polystyrene standard): M_w = 11,000 Da, M_n = 6,200 Da, and PDI = 1.7.

UV-vis ($CHCl_3$): 416, 678 nm.

Funding Information

We gratefully acknowledge financial support from SERB, India (SERB/SRG/2021/000648) for funding this research.

Acknowledgment

High Performance Computing Centre, SRM Institute of Science and Technology is acknowledged for providing the computational facility.

Supporting Information

Supporting Information for this article is available online at https://doi.org/10.1055/s-0042-1757979.

References

(1) New address: Department of Radiology, University of Texas Southwestern Medical Center, Dallas, TX 75390, USA.
(2) New address: Institute of Chemistry, The Hebrew University of Jerusalem, Edmond J. Safra Campus, Jerusalem, 91904, Israel.
(3) New address: Department of Chemistry, Dhemaji College, Dibrugarh University, Dhemaji, Assam, 787057, India.
(4) Guo, X.; Baumgarten, M.; Müllen, K. *Prog. Polym. Sci.* **2013**, *38*, 1832.
(5) Qiu, Z.; Hammer, B. A. G.; Müllen, K. *Prog. Polym. Sci.* **2020**, *100*, 101179.
(6) Fratini, S.; Nikolka, M.; Salleo, A.; Guillaume, S.; Sirringhaus H. *Nat. Mater.* **2020**, *19*, 491.
(7) (a) Qiang, P.; Sun, Z.; Xue, B.; Zhang, F. *Org. Mater.* **2021**, *3*, 221. (b) Weldeab, A. O.; Kornman, C. T.; Li, L.; Starkenburg, D. J.; Zhao, X.; Fagnani, D. E.; Sadovy, S. J.; Perry, S. S.; Xue, J.; Castellano, R. K. *Org. Mater.* **2021**, *3*, 390. (c) Cao, X.; Min, Y.; Tian, H.; Liu, J. *Org. Mater.* **2021**, *3*, 469. (d) Chaudhuri, D. *Org. Mater.* **2021**, *3*, 455. (e) Ávila-Rovelo, N. R.; Ruiz-Carretero, A. *Org. Mater.* **2020**, *2*, 47.
(8) (a) Advincula, A. A.; Jones, A. L.; Thorley, K. J.; Österholm, A. M.; Ponder Jr., J. F.; Reynolds, J. R. *Chem. Mater.* **2022**, *34*, 4633. (b) Dyer, A. L.; Thompson, E. J.; Reynolds, J. R. *ACS Appl. Mater. Interfaces* **2011**, *3*, 1787. (c) Kim, J.; Rémond, M.; Kim, D.; Jang, H.; Kim, E. *Adv. Mater. Technol.* **2020**, *5*, 1900890.
(9) Gibson, G. L.; McCormick, T. M.; Seferos, D. S. *J. Am. Chem. Soc.* **2012**, *134*, 539.
(10) (a) Zhang, Q.; Tsai, C.-Y.; Li, L.-J.; Liaw, D.-J. *Nat. Commun.* **2019**, *10*, 1239. (b) Li, K.; Zhang, Q.; Wang, H.; Li, Y. *ACS Appl. Mater. Interfaces* **2014**, *6* 13043.
(11) Zhu, C.; Meng, L.; Zhang, J.; Qin, S.; Lai, W.; Qiu, B.; Yuan, J.; Wan, Y.; Huang, W.; Li, Y. *Adv. Mater.* **2021**, *33*, 2100474.
(12) Hu, Z.; Huang, Q.; Liu, C.; Song, A.; Shao, L.; Bai, Y.; Hu, Z.; Zhang, K.; Huang, F.; Cao, Y. *Org. Mater.* **2022**, *4*, 18.
(13) Das, S.; Pati, P. B.; Zade, S. S. *Macromolecules* **2012**, *45*, 5410.
(14) Bedi, A.; Senanayak, S. P.; Das, S.; Narayan, K. S.; Zade, S. S. *Polym. Chem.* **2012**, *3*, 1453.
(15) (a) Bedi, A.; Senanayak, S. P.; Narayan K. S.; Zade, S. S. *Macromolecules* **2013**, *46*, 5943. (b) Bedi, A.; Debnath, S.; Chandak, H. S.; Zade, S. S. *RSC Adv.* **2014**, *4*, 35653.
(16) (a) Luppi, B. T.; McDonald R. Ferguson, M. J.; Sang L.; Rivard, E. *Chem. Commun.* **2019**, *55*, 14218. (b) He, G.; Delgado, W. T.; Schatz, D. J.; Merten, C.; Mohammadpour, A.; Mayr, L.; Ferguson, M. J.; McDonald, R.; Brown, A.; Shankar, K; Rivard, E. *Angew. Chem. Int. Ed.* **2014**, *53*, 4587.
(17) Das, S.; Bedi, A.; Krishna, G. R.; Reddy, C. M.; Zade, S. S. *Org. Biomol. Chem.* **2011**, *9*, 6963.
(18) Bedi, A.; Senanayak, S. P.; Narayan, K. S.; Zade, S. S. *Macromolecules* **2013**, *46*, 5943.
(19) Bedi, A.; Senanayak, S. P.; Das, S.; Narayan, K. S.; Zade, S. S. *Polym. Chem.* **2012**, *3*, 1453.
(20) Debnath, S.; Singh, S.; Bedi, A.; Krishnamoorthy, K.; Zade S. S. *J. Phys. Chem. C* **2015**, *119*, 15859.
(21) Das, S.; Senanayak, S. P.; Bedi, A.; Narayan, K. S.; Zade, S. S. *Polymer* **2011**, *52*, 5780.
(22) Bedi, A.; Senanayak, S. P.; Narayan, K. S.; Zade, S. S. *J. Polym. Sci., Part A: Polym. Chem.* **2013**, *51*, 4481.
(23) Gaupp, C.L.; Welsh, D.M.; Reynolds, J. R. *Macromol. Rapid Commun.* **2002**, 23, 885.
(24) Naik, M. A.; Venkatramaiah, N.; Kanimozhi, C.; Patil, S. *J. Phys. Chem. C* **2012**, *116*, 26128.
(25) (a) Kanimozhi, C.; Yaacobi-Gross, N.; Chou, K. W.; Amassian, A.; Anthopoulos, T. D.; Patil, S. *J. Am. Chem. Soc.* **2012**, *134*, 16532. (b) Xu, Z.; Hou, S.; Zhu, Z.; Zhou, P.; Xue, L.; Lin, H.; Zhou, J.; Zhuo, S. *Nanoscale* **2021**, *13*, 2673. (c) Wang, Y.; Hamidi-Sakr, A.; Surgailis, J.; Zhou, Y.; Liao, H.; Chen, J.; Zhu, G.; Li, Z.; Inal, S.; Yue, W. *J. Mater. Chem. C* **2021**, *9*, 13338.
(26) Maity, S.; Bedi, A.; Patil, S. *J. Polym. Sci.* **2021**, *59*, 3181.

(27) Mukhopadhyay, T.; Puttaraju, B.; Senanayak, S. P.; Sadhanala, A.; Friend, R.; Faber, H. A.; Anthopoulos, T. D.; Salzner, U.; Meyer, A.; Patil, S. *ACS Appl. Mater. Interfaces* **2016**, *8*, 25415.
(28) Chen, X.; Qiao, W.; Wang, Z. Y. *RSC Adv.* **2017**, *7*, 15521.
(29) Singh, S.; Chithiravel, S.; Krishnamoorthy, K. *J. Phys. Chem. C* **2016**, *120*, 26199.
(30) Debnath, S.; Boyle, C. J.; Zhou, D.; Wong, B. M.; Kittilstved, K. R.; Venkataraman, D. *RSC Adv.* **2018**, *8*, 14760.
(31) The UV-vis spectra can be reliably recorded only up to 1600 nm in our current instrument.
(32) Bedi, A.; Zade, S. S. *Macromolecules* **2013**, *46*, 8864.